Optimization of High-order Harmonic Generation using an Ultrashort Pulse High-Intensity Laser

Report
by
Bernd Schütte

Lund Reports on Atomic Physics, LRAP-360
Lund, May 2006

Abstract

High-order harmonic generation is studied mainly in Argon using the Terawatt Laser System in Lund that provides short pulses. After giving an introduction of the setup, the underlying principles of high-order harmonic generation are described. The experiments were done changing a set of parameters and taking a large amount of harmonic spectra. A detailed study of double peaks occurring was made linking them to the short and long trajectories. It is shown that it is possible to choose one of the double peaks by setting the right experimental conditions. Further, a tunability of the harmonics was proved. Towards a higher efficient and more tunable harmonic generation process, the alignment of a parabolic mirror is described.

Contents

Chapter 1

Introduction

Since the first working laser was built by Theodore H. Maiman in 1960, lasers have become ubiquitous, finding utility in highly varied applications in every section of modern society including science, medicine, industry, information technology, consumer electronics and the military.

Light that is emitted by a laser has significant different properties in comparison to light that is emitted by a natural source. Among these are coherence, directionality, brightness and for some lasers a very short pulse duration. In order to extend these properties to shorter wavelengths, High-order Harmonic Generation (HHG) plays an important role.

1.1 Background and Motivation

The process of generating harmonics was discovered only one year after the invention of the laser, when second-harmonic radiation was obtained [1]. But from then it took another 26 years until 1987, when High-order Harmonic Generation was observed for the first time [2]. HHG is a nonlinear optical effect that occurs when an intense laser beam is interacting with free atoms. In order to achieve the needed intensities for HHG, the laser beam has to have a high energy and a short pulse duration. During the process a discrete spectrum of ultraviolet and x-ray radiation is produced with frequencies that correspond to odd multiples of the incident laser frequency. The harmonic spectrum is characterized by a strong decrease in intensity for the first few orders, after which a plateau is formed by harmonics with approximately the same intensity. This plateau ends in a sharp cutoff. Each harmonic radiation pulse is spatially and temporally fully coherent.

The intensities of harmonic radiation achieved today are quite low and have to be increased. Very short and intense x-ray pulses would open up new possibilities for time-resolved structural imaging in biology. In the past synchrotrons have provided x-ray beams, but in research areas like structural biology much shorter pulses with much higher energy than delivered by synchrotrons are required. On the other hand, Free Electron Lasers will provide a source of ultra-intense x-ray beams in a few years, but the

access to these facilities will be very limited and connected with tremendous costs [3]. High-order Harmonic Generation followed by subsequent amplification in a laser plasma offers an excellent potential to provide a new ultra-intense soft x-ray source adapted to biology and complementary fields.

For applications it might be desirable to choose particular wavelengths of the x-ray radiation. That is why also a tunability of the discrete harmonic spectrum is needed. In order to reach these two goals, new methods have to be developed. This project deals with a detailed analysis of harmonic spectra while changing several parameters in the HHG process. This gives the basis for further improvements in the setup in order to achieve tunability of the radiation combined with a high intensity.

1.2 Outline

Chapter 2 gives an overview about the Terawatt Laser in Lund as well as a detailed description of the experimental setup used for HHG. The theory of the harmonic generation process is presented in chapter 3. This aims, however, more at an intuitive understanding of the main aspects involved in HHG rather than giving detailed mathematical derivations. Chapter 4 discusses the results for each parameter that has been varied, while the last chapter contains the conclusions that can be drawn from the work carried out and gives a short outlook.

Chapter 2

The Experimental Setup

This chapter gives an overview of the laser system and of the various components used in order to generate and detect harmonics. The experiments were performed in a special target room where the laser beam could be sent in.

2.1 The Multi-Terawatt Laser System in Lund

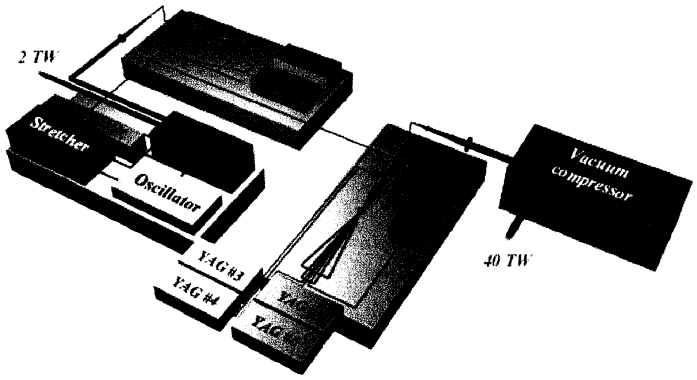

Figure 2.1: Schematic of the Terawatt Laser System

A high-power laser facility generating very short pulses was established at the Lund Laser Centre (LLC) in 1992. Titanium doped Sapphire is used as the active medium and after amplification laser pulses with a repetition rate of 10 Hz are emitted [4]. Since 1992 the laser system has been upgraded several times and is now able to generate pulses with a pulse duration (FWHM) down to 35 fs. Pulses can now be amplified to an energy of about 1.4 J corresponding to a peak power of 40 TW [6]. The beam that we used for our experiment had a pulse energy of a few tens of mJ.

Figure 2.1 shows a schematic of the laser system. An Ar-ion pumped Ti:Sapphire oscillator produces 20 fs short pulses with a repetition rate of 80 MHz. Of these 10 pulses per second are being amplified in different amplifier stages using the method of Chirped Pulse Amplification (CPA) that will be described below. Nd:YAG lasers #1 and #2 are used to longitudinally pump the crystal in the amplifier from both sides. After the multipass amplifier the beam is compressed and used in particular to generate harmonics [6].

2.1.1 Chirped Pulse Amplification

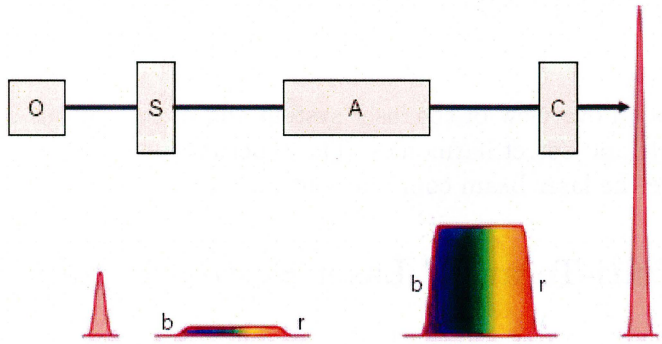

Figure 2.2: Principle of Chirped Pulse Amplification

The method of Chirped Pulse Amplification is used in order to produce very high laser intensities. Figure 2.2 shows the basic principle of CPA, where the oscillator output (O) is stretched in the stretcher (S) such that the red frequency components (r) travel ahead of the blue (b). The peak intensity is reduced in this process. The stretched pulse is then amplified in a multipass amplifier (A) before recompression in a grating-pair compressor (C). By this method the optics are protected from being damaged, while achieving large pulse energies.

Furthermore the way of recompressing a pulse offers a possibility to influence the generation of harmonics. If the pulse is not compressed to its minimum in pulse duration, it will be chirped. Thus either the red frequency components arrive before the blue ones referring to a positive chirp, or the blue ones arrive earlier referring to a negative chirp. Changing the distances between the gratings results in a pulse that is either positively or negatively chirped or without any chirp.

2.1.2 Mode locking

The generation of very short pulses is achieved by mode locking. If the phase difference between consecutive longitudinal modes oscillating in a laser cavity is constant, very short pulses are formed in the time domain. For a Gaussian pulse the following equation

is valid: $\Delta\tau = 0.441/\Delta\nu$ [7], where $\Delta\tau$ is the pulse duration (FWHM) and $\Delta\nu$ the bandwidth of the laser. Thus a short pulse corresponds to a large bandwidth. For example pulses of 20 fs duration will lead to a bandwidth of about 50 nm.

The mode locking method used in the Terawatt Laser in Lund is Kerr-lens mode locking. This is a passive technique and is based on the optical Kerr effect. For very high intensities, the Ti:Sapphire crystal will act as a lens due to self-focusing. If some modes incidentally are phase locked and interfere constructively forming a pulse that has higher intensity than the modes with random phases, this pulse is focused and thereby collimated due to the Kerr effect, while the modes with random phases are not focused. The unfocused light can thus be blocked with an appropriate aperture and suffers from losses. The modes in phase will be increased in intensity until only a very short pulse with a high intensity survives.

2.2 Experimental setup for harmonic generation

2.2.1 General setup using a focusing lens

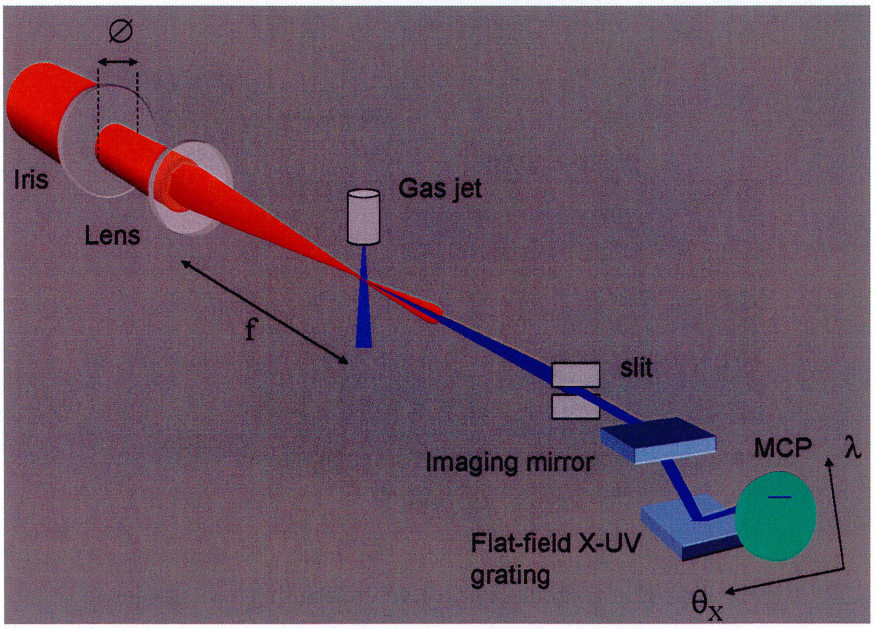

Figure 2.3: General setup for HHG

A schematic of the setup for generating harmonic radiation is shown in figure 2.3. The incoming laser beam has a diameter of approximately 4 cm and is first cut by an iris in order to get a defined and variable beam size in the order of 1 to 2 cm. Afterwards the beam is focused by a planoconvex lens with a focal length of 2 m. The convex side

hereby faces the incoming beam to reduce aberrations and get a diffuse back reflection. The lens is mounted on a translation stage in order to move the focus with respect to the gas jet. Thus the focal plane can be moved either to a position that corresponds to the middle of the gas jet, a few cm before or a few cm after it. With the help of two stirring mirrors that are not shown in the figure, the beam can be aligned on an optical axis, defined by two points. The lens is installed after this alignment and adjusted by making both the focused laser beam and the back-reflected light coincide with the optical axis.

2.2.2 Gas Jet

Argon was mainly used for the experiments, but some of the measurements were performed with Neon. The gas is supplied by a pulsed piezoelectric valve that is depicted in figure 2.4. Using a jet nozzle, the gas is shot from above to the laser beam and has a diameter in the order of 1 mm. The jet is triggered by an input signal coming from the laser in order to obtain a maximum density of the gas during the laser pulse. This also has the advantage that the background pressure in the chamber is not increased too much. The nozzle position can be adjusted by micrometer screws in three directions to properly hit the medium with the laser pulses. The laser beam is supposed to be close to the jet nozzle, where the radius of the gas jet is the smallest and thus the density the highest.

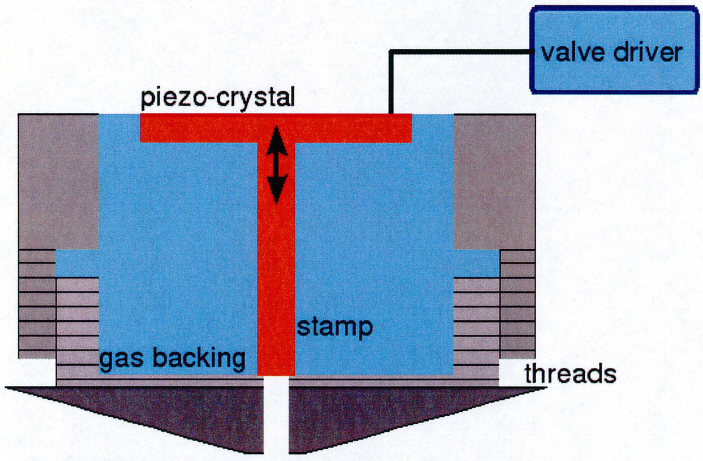

Figure 2.4: The piezoelectric valve controlling the gas jet [6]

2.2.3 Vacuum System

After focusing by the lens the beam enters a tube and travels in vacuum. This is necessary because the intensity of the beam increases by getting focused. Thus nonlinear optical effects like self-phase-modulation and self-focusing would occur when traveling

in air. The beam profile would be distorted and the conditions for HHG deteriorated. Furthermore the generated harmonic radiation has to be kept in vacuum in order not to get absorbed by the air. Finally, the MCP is to be pumped to a very low pressure of 10^{-5} mbar in order to purge it.

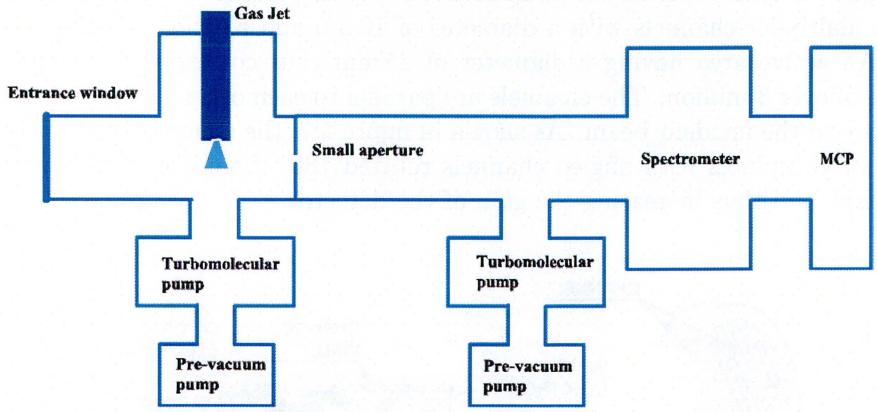

Figure 2.5: Schematic of the vacuum system

Figure 2.5 shows a schematic of the vacuum chambers that are pumped by two different systems, each consisting of a pre-vacuum pump and a turbomolecular pump. One system pumps directly under the gas jet to reduce the background pressure due to the pulsed noble gas. The pressure in this chamber when the pulsed valve is operating, reaches a value of about 10^{-4} mbar. The other system is pumping before the spectrometer in order to get the lowest possible pressure where the MCP is placed. The pressure here has to be not more than about 10^{-5} mbar and drops to values under 10^{-6} mbar after several hours of pumping. A small aperture is inserted directly after the chamber with the gas jet in order to minimize gas flow to the second vacuum part.

2.2.4 Spectrometer

The spectrometer is an I.S.A. Jobin-Yvon PGM PGS 200. An entrance slit with an aperture of about 1 cm in the horizontal direction selects part of the radiation. The aperture in vertical direction can be varied from 0 to 2 mm. For the experiments a value of 200 μm is appropriate. The infrared laser beam and the generated harmonics propagate in the same direction and have to be separated. Moreover one wants to separate the different harmonic orders. Therefore the light is focused by a toroidal mirror onto a plane platinum grating that has 450 grooves per mm and separates different wavelength components. It gives optimal results for the wavelength region from 16 nm to 80 nm. The position of the grating can be moved in order to detect different parts of the spectrum. In principle the fundamental beam can be seen as well, but under the condition for observing harmonics it is reflected at quite a large angle.

2.2.5 Detection

Connected to the spectrometer microchannel plates (MCP) are used as a detector. The MCP used for our experiments is an Advanced performance Chevron. It is similar to an electron multiplier and appropriate to detect VUV and x-ray radiation. On the left side of figure 2.6 the structure of an MCP is shown. It consists of an array of miniature electron multiplier channels with a diameter of $10\,\mu$m and a spacing of $12\,\mu$m between them. An active area having a diameter of 25 mm thus corresponds to a number of channels of over 3 million. The channels are parallel to each other and are at an angle of $8\,^\circ$ relative to the incident beam. As shown in figure 2.7, the Chevron assembly actually consists of two plates with angled channels rotated $180\,^\circ$ from each other producing a v-like shape and thus increasing the gain of the detector.

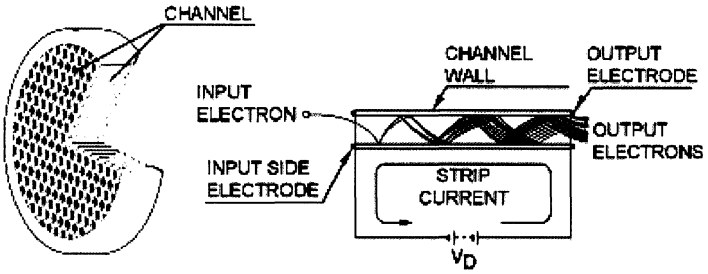

Figure 2.6: Schematic of a microchannel plate

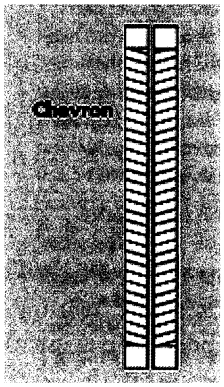

Figure 2.7: Chevron consisting of two microchannel plates

A voltage of usually $V_{MCP} = -1500\,\mathrm{V}$ is applied to the MCP. A single electron or photon interacting in a channel of the MCP produces a charge pulse of about 1000 electrons that emerge from the rear of the plate. This process is illustrated on the

right side of figure 2.6. The electrons that exit the first plate then start a cascade of electrons that propagate through the second plate. After propagating through the two plates the electrons experience an acceleration voltage of usually $V_{Ph} = 3200\,\mathrm{V}$ towards a phosphor screen. Both voltages applied to the detector are controlled by high-voltage power supplies. After hitting the screen the electrons emit visible phosphorescent light. A CCD camera of the type Marlin F-033B/C consisting of 656×494 pixel records the phosphor screen. It is triggered by a signal from the laser and the images are transferred to a computer. We usually worked with a recording time of 60 ms and accumulated 40 single pictures.

2.2.6 Focusing with a parabolic mirror

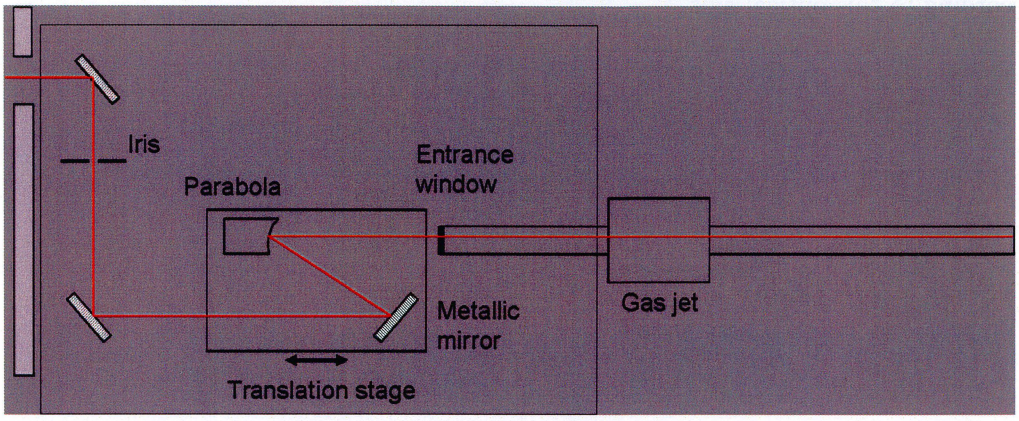

Figure 2.8: Setup using a parabolic mirror

A series of measurements were performed with a parabolic mirror with 1 m focal length. The advantage of using a mirror instead of a lens is that the focusing is independent of wavelength. This offers the possibility to do experiments with laser light consisting of different spectral distributions. Furthermore, the temporal distortion is decreased.

The parabolic mirror is designed for an incident angle of 12.3°. Therefore another mirror has to be used in order to be able to send the beam through the gas jet. A positioning as shown in figure 2.8 is appropriate. The distance between the metallic mirror and parabola has to be kept constant so that both mirrors have to be mounted on a translation stage. The translation stage makes it possible to move the focus of the laser beam with respect to the gas jet.

It is helpful to start the alignment using as HeNe laser instead of using the infrared beam, because it has a better beam profile and is easier to handle. The metallic mirror and the parabola have to be put to an angle and a position so that the beam before the metallic mirror and after the parabola are roughly parallel. However, in order to

do a precise alignment, it is very useful to work with a Phasics, i.e. a camera using lateral shearing interferometry. With this instrument it is possible to measure wavefront distortions like astigmatism. The Phasics should be put once before focusing and once after focusing. By putting the Phasics after the focus and changing slightly the tilt of the parabola, the wavefront of the beam can be optimized.

This procedure has to be done again when working with the infrared beam. An important requirement is that the beam position and direction after focusing are not changing while moving the translation stage. This is achieved by observing the beam at a point after the focus, moving the translation stage and correcting with the tilts of the parabola and the metallic mirror. Separate translations for both mirrors can also be helpful. After this procedure the values of the wavefront distortions have to be checked with the Phasics again. It is important to notice that a new optical axis should be defined after the preceding alignment and all other parts of the setup should be adjusted according to this optical axis.

Chapter 3

Theory of Harmonic Generation

This chapter will briefly explain the process of high-order harmonic generation within the semiclassical model that shows a large part of the harmonic properties. A full description, however, requires a quantum mechanical treatment that is beyond the scope of this report. For more detailed treatments see [8] and [9].

3.1 Atoms in strong fields

High-order harmonic generation originates from the interaction of atoms with the strong electromagnetic fields produced by focused laser light. In order to get an idea of the magnitude of the needed intensities, we make simple estimates. An electron in the ground state of a hydrogen atom experiences a Coulomb field equal to $5 \times 10^9\,\mathrm{V/cm}$. The laser intensity I that would be needed in order to reach the same value of the electric field can be calculated by

$$I = \frac{1}{2}\epsilon_0 c\,|E|^2\,, \tag{3.1}$$

where ϵ_0 is the permittivity of vacuum and c the speed of light. This gives an intensity of $3.5 \times 10^{16}\,\mathrm{W/cm^2}$ which often is referred to as the atomic unit of intensity. If an atom is exposed to such a field, the electron can overcome the Coulomb field and thus the atom will be ionized. However, the values for the intensity produced by lasers used for HHG reach values in the order of 10^{14} to $10^{15}\,\mathrm{W/cm^2}$ thus being just a fraction of the atomic unit of intensity. Still ionization can occur and three mechanisms can be considered depending on the laser intensity and frequency as well as on the ionization potential of the gas medium. Figure 3.1 shows the different regimes for ionization processes.

When the intensity is relative low, **multiphoton ionization (MPI)** will occur (figure 3.1a). In this case several photons interact with the atom at the same time, providing the necessary energy to overcome the binding energy and releasing the electron to the continuum. This process often described by perturbation theory dominates for intensities below $\approx 10^{14}\,\mathrm{W/cm^2}$, for the laser frequency used in the experiments.

A higher intensity enables the field to distort the Coulomb potential and thus increase the probability for the electron to tunnel through the barrier formed by the suppressed

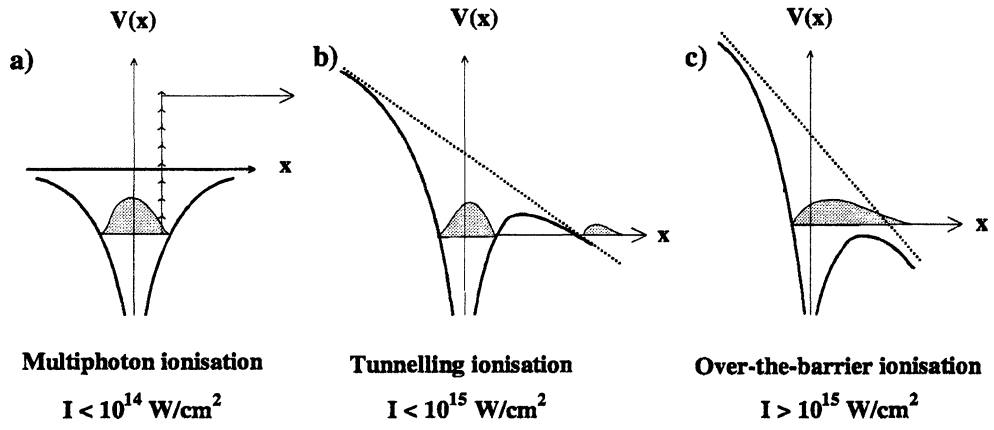

Figure 3.1: Different ionization mechanisms for an atom in a laser field. In (a) multiphoton ionization dominates. As the intensity decreases (b) the Coulomb potential is distorted and the electron can tunnel through the barrier. As the intensity is further increased (c) the whole wave packet can escape, due to the barrier being suppressed [9].

atomic potential (figure 3.1b). The atom gets ionized by **tunnel ionization**. It is expected to be dominant in a region of intensities from about 10^{14} to $10^{15}\,\mathrm{W/cm^2}$.

When the intensity gets bigger the barrier gets lower and finally the ground state is no longer bound (figure 3.1c). This is true for intensities above $10^{15}\,\mathrm{W/cm^2}$ and is known as **over-the-barrier ionization**.

3.2 Physics of High-order Harmonic Generation

Low-order harmonic generation up to the 5^{th} or 7^{th} order can happen even for relatively low fields. It is then described by lowest order perturbation theory.

3.2.1 The 3-step model

HHG, however, cannot be understood with perturbation theory, since the intensity of harmonics in the so called plateau region does not decrease with increasing order. In fact, HHG occurs when atoms get ionized by tunnel ionization. A semiclassical model has been developed which gives a fairly intuitive understanding of the HHG process. Semiclassical here means that the electron is partly described as a classical particle. Furthermore the atom is supposed to have only one active electron. According to this model, harmonic generation occurs in three steps that are illustrated in figure 3.2.

(i) The atom is ionized by the tunnel ionization process.

(ii) The free electron is accelerated away from the atom by the electric field. When the electric field changes sign, there is a force in the opposite direction and the electron has the possibility to return to the vicinity of the atom again.

(iii) When the electron is close to the atom there is a certain probability for recombination back to the ground state. The captured electron emits all its kinetic energy plus the ground state binding energy I_p as a photon.

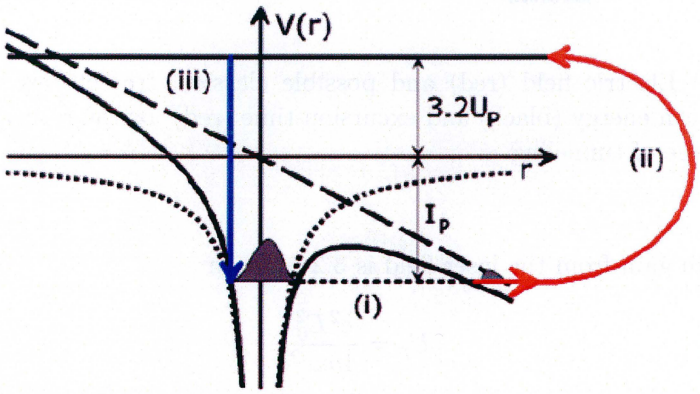

Figure 3.2: The 3-step model. The undisturbed Coulomb potential is in dotted line, the electric field potential at one instant in time is in dashed line and the combined potential in solid line [8].

The model implies that the laser light needs to be linearly polarized. Otherwise the electron would not be accelerated back towards the atom with a significant probability.

The process is periodic in time, because the electron tunnels out when the electric field is close to its maximum. Due to the periodicity in time there is also a periodicity in frequency leading to the orders of harmonic generation. Since the gas is isotropic, there is no difference in the case the electron tunnels out when the electric field is $-E$ or E. Thus the period time of the process is actually $T/2$ where T is the laser period. Transformed to the frequency domain, this means that if the laser frequency is ω, then the emitted radiation occurs with a periodicity of $2\,\omega$. Regarding the fundamental laser frequency as the first order, only odd harmonics will be observed [10].

It turns out that only for certain release times the electron can return to the atom, for other times it drifts away. The harmonic emission occurs dominantly when the electron is released just after the peak of the field oscillation, and returns between a half and a full laser period later. The energy gained by the electron and hence the energy of the emitted photon, depends on the time of tunneling and the time of recombination, i.e. the phase of the electric field at those times. The maximum kinetic energy that an electron

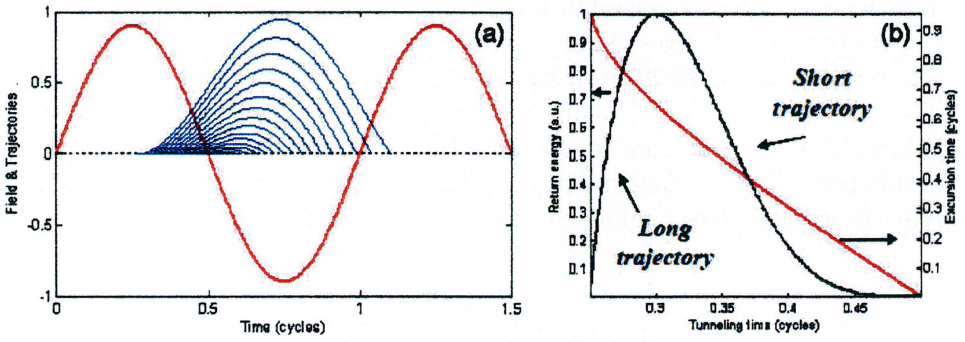

Figure 3.3: (a) Electric field (red) and possible classical trajectories of the electron (blue). (b) Return energy (black) and excursion time (red) for the returning electron as a function of time of tunneling.

theoretically can gain from the laser field is 3.2 U_p with

$$U_p = \frac{e^2 E_0^2}{4m\omega^2}. \tag{3.2}$$

Here e is the electron charge, E_0 is the amplitude of the electric field and m is the electron mass. U_p is called the ponderomotive energy and refers to the average energy an electron can gain in an electric field. The maximum photon energy is

$$E_f = I_p + 3.2U_p. \tag{3.3}$$

E_f corresponds to the cut-off energy of the harmonic spectrum meaning that no radiation with a higher energy will be observed. Below this value, however, all possible recollision energies have roughly the same probability leading to a long plateau of peaks with nearly equal amplitude.

3.2.2 The long and the short trajectory

As mentioned before, the energy gained by an electron that is accelerated in a field using a simple classical picture, depends on the tunneling time. Figure 3.3a shows different possible electron trajectories. The first electrons are ionized directly after the maximum of the field and have the longest excursion times. In a quantum mechanical description the single electron does not follow a single trajectory and instead one has to think of an electron packet that is distributed over the different trajectories.

Figure 3.3b shows the time the electron has been away from the atom referred to as excursion time, and that is decreasing for increasing tunneling times. Furthermore a plot of the return energy over the time of tunneling is depicted. An electron that is tunneling 0.3 optical cycles after the zero of the electric field (see figure 3.3b) will

have the maximum of energy when it finally recombines with its parent ion. Figure 3.3b shows also that each specific energy can be obtained on two different trajectories. These trajectories are distinguished by their excursion times and are thus called the long and the short trajectory.

In general the properties of the emitted light pulse are directly linked to those of the recolliding electron wave packet, making it crucially dependent on the electron dynamics in the continuum. This means that the emitted light pulses according to the two trajectories have significant different properties due to the different long excursion times.

3.2.3 Phase matching

Phase matching is a particularly important aspect of harmonic generation. If the condition of phase matching is fulfilled, it means that the difference in phase between the induced polarization and the generated field is minimized over the medium length. Thus an efficient energy transfer from the laser field to the harmonics is achieved. A useful parameter characterizing phase matching is the coherence length L_{coh} that defines a length over which the generated field and the polarization induced experience a phase difference of π.

There are essentially three contributions that can introduce a phase shift between the incoming laser light and the generated harmonics. **Dispersion** makes different frequencies travel with different velocities so that they get out of phase with each other. The **Gouy phase shift**, which comes into play when a laser beam is going through a focus, induces a geometrical phase mismatch. By using a loose focus and a short medium, this kind of phase mismatch can be minimized. Finally, the **intensity dependence of the harmonic dipole phase** also leads to an atomic phase mismatch. Theoretical studies of HHG by a single atom exposed to an intense laser field have shown that the dipole phase varies rapidly as a function of the laser intensity, especially for the long trajectory. Thus the phase will be different for different atoms in the interaction volume, since the laser intensity varies strongly both in time and space in the medium [9].

The long and the short trajectory that were discussed before both contribute to the harmonic dipole moment with a term characterized by a phase, Φ_i, which is given by the action along the considered electron trajectory and turns out to be proportional to the intensity of the driving laser field:

$$\Phi_i(t) = -\alpha_i I(t) \tag{3.4}$$

The intensity dependent phase gives rise to spectral broadening and chirp of each harmonic. The coefficients α_l and α_s are different for the long and short paths and closely related to the time spent by the electron in the continuum. A longer excursion time corresponds to a larger value of the α coefficient. The spectral content and chirp of the harmonic will be quite different depending on which trajectory is dominant. The intensity varies over the pulse not only temporally, but also spatially. The radial variation $I(r)$ will affect the curvature of the phase front of the harmonics, thus determining the

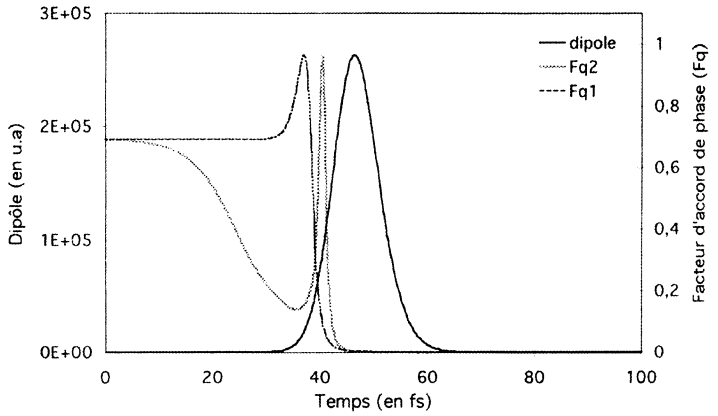

Figure 3.4: Evolution in time of the dipole moment and the phase matching factors for the short (Fq1) and long (Fq2) trajectory contributions [12]

divergence of the emitted beam. The short trajectory will be associated with a small divergence, whereas the long trajectory leads to a large divergence [11]. The total electric field of the generated harmonics can be modelled as

$$E = E_l e^{-i\alpha_l I} + E_s e^{-i\alpha_s I}, \tag{3.5}$$

where E_l and E_s are the electric fields corresponding to the long and short trajectories, respectively. The square of the electric field then gives the intensity of the harmonics.

Figure 3.4 depicts a simulation that is taken from [12]. It shows the time evolution of the single atom dipole moment together with the 'phase matching factor' for the short and long trajectories for the 23^{rd} harmonic in Argon, a pulse duration of 30 fs and an intensity of $3 \times 10^{14}\,\mathrm{W}/\mathrm{cm}^2$. Under these conditions the contribution due to the long trajectory is clearly produced after that of the short trajectory.

3.2.4 Influence of the gas medium

The noble gases are experimentally the most suitable elements and Xenon, Krypton, Argon, Neon and Helium have traditionally been used. Of these Helium has the highest ionization potential (I_p), allowing the atom to be exposed to high intensities before being ionized. Equation 3.3 thus shows that it is possible to generate harmonics with much higher orders for Helium than e.g. for Xenon. On the other hand the conversion efficiency is much higher for the gases with lower ionization potentials leading to stronger harmonic peaks. It can be added that in general the conversion efficiency - i.e. the fraction of intensity of the laser beam being transformed into harmonic radiation - has a very low value of $\approx 10^{-6}$.

Chapter 4

Experimental Results

This chapter will provide an overview of the experimental data along with possible interpretations. First the experimental conditions such as pulse duration and pulse energy after compression will be described. Then different harmonic spectra taken under different conditions will be shown. However, the amount of data taken is very large so that only a selection can be considered here.

4.1 Experimental conditions

4.1.1 Pulse duration

As mentioned in chapter 2, the laser pulses can have a duration down to 35 fs. However, depending on the settings of one of the gratings in the compressor, the pulses get chirped and thus elongated in time. In order to investigate how the pulse duration is changing for different compressor settings, an autocorrelator was used. The beam is sent into the autocorrelator and split into two equally strong pulses, which are delayed by propagating different paths in the two arms of the autocorrelator. The beams finally cross each other in a frequency-doubling crystal emitting frequency-doubled light whose spatial distribution is dependent on the temporal overlap of the two pulses. By changing the path differences for the two beams and observing the spatial distribution of the emitted light, the instrument can measure the pulse duration.

Figure 4.1 shows the result. The grating position referred to as L in this report is displayed in mm corresponding to a specific value for the distance between the gratings. Increasing values of L here correspond to decreasing values for the distance. One can see that there is a minimum in pulse duration for a grating position of about 5.6 mm referred to as the best compression. The pulse duration for this compressor setting is approximately 40 fs. A grating position larger than about 5.6 mm corresponds to a pulse with a positive chirp, while a smaller value introduces a negative chirp. The variation of the pulse duration around the best compression is roughly symmetric.

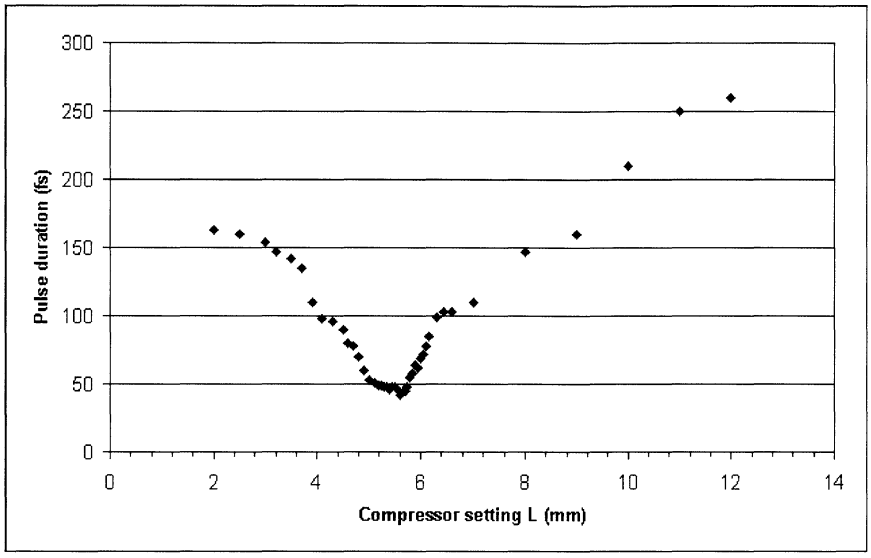

Figure 4.1: Pulse duration as a function of the grating position (chirp)

4.1.2 Pulse energy

The pulse energy is approximately 200 mJ before compression, but it is reduced after going through the compressor. Only a fraction of it is used for HHG. The energy of the beam was measured after propagating through the iris, the lens and the entrance window of the vacuum chamber. This was done for different iris diameters, and the result can be seen in figure 4.2. Although the area of the beam that is transmitted, increases quadratically with increasing iris diameter, the energy does not. This is because the beam intensity is maximal at the center of the beam profile.

4.1.3 Conversion efficiency

Figure 4.3 shows the fraction of intensity converted into the radiation of different harmonic orders. This measurement was performed using a photodiode that was located about 1 m after the focal point. It measures the intensity of the complete harmonic spectrum so that the relative strengths of the different orders have to be deduced by analyzing an integrated spectrum. Furthermore an aluminium filter has to be put in in order to block the infrared beam. Thus the energy measurement has to be corrected taking into account the transmission coefficients for each harmonic. This was done for a special setting with values for the iris diameter of $\varnothing = 15\,\text{mm}$, the compressor setting of $L = 5.6\,\text{mm}$ (best compression) and a lens position of $z = 0\,\text{cm}$ which means that the focus is at the gas jet. As pointed out before, the conversion efficiency is low and reaches a maximum for the 25^{th} order. For other settings, however, this might give different results.

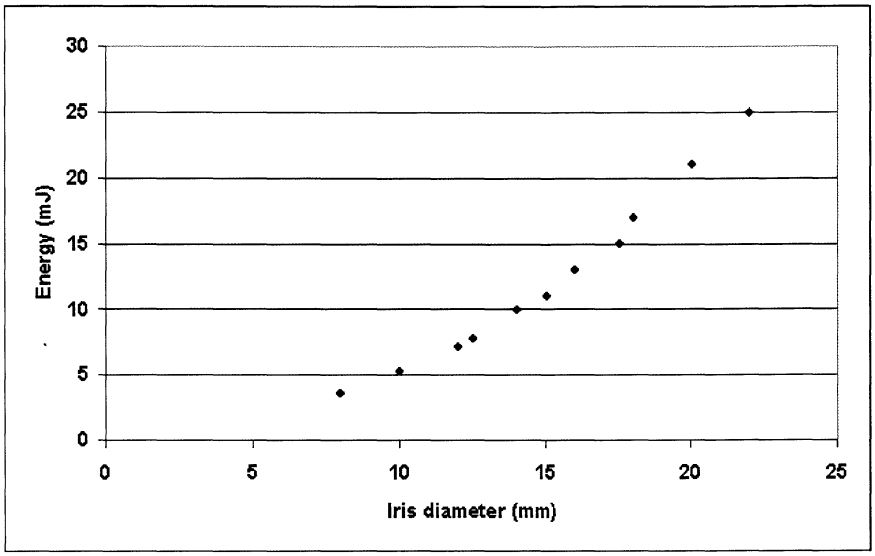

Figure 4.2: Energy of the laser pulses after compression

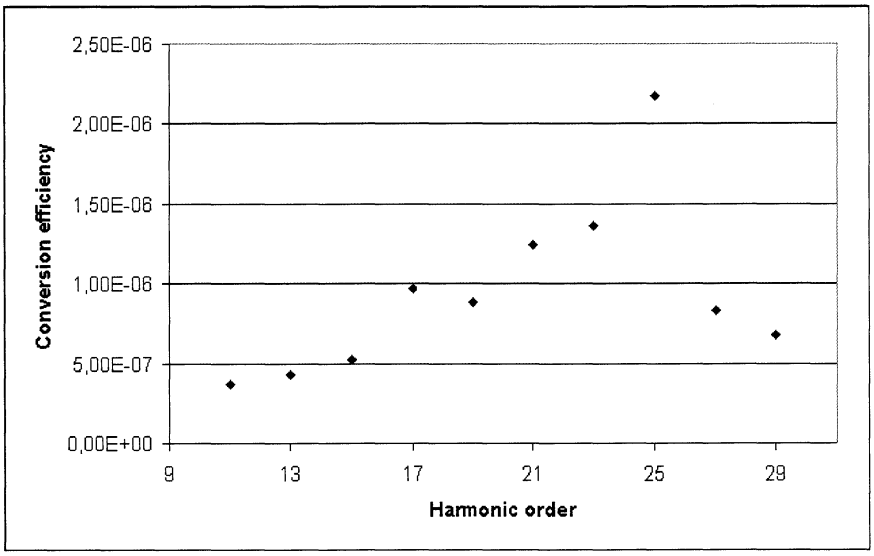

Figure 4.3: Conversion efficiency

4.2 Harmonic spectra

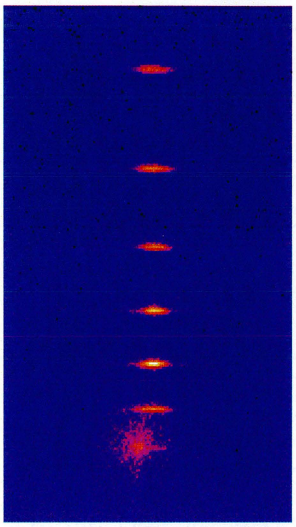

Figure 4.4: Harmonic spectrum

A typical harmonic spectrum is depicted in figure 4.4. As shown in figure 2.3, the vertical direction corresponds to a wavelength with increasing wavelength to the upper side. The horizontal direction refers to the divergence of the beam. This spectrum is taken for $\varnothing = 10\,\text{mm}$, $z = 0\,\text{cm}$ and $L = 4.8\,\text{mm}$ and shows the harmonic orders from 15 to 27. The calibration was done by plotting the peak positions over different series of the inverse of harmonic orders with the series giving the best line being the actual harmonic orders. At the bottom of figure 4.4 the 27^{th} order can be seen weakly on the right side. The diffuse light left to it comes from lower harmonic orders that are entering the spectrometer through another hole than the entrance slit and going through without hitting the toroidal mirror and the grating.

Figure 4.5 depicts another harmonic spectrum that is taken for $\varnothing = 15\,\text{mm}$, $z = 0\,\text{cm}$ and $L = 4.4\,\text{mm}$. It shows a striking feature that each harmonic order actually consists of two well separated peaks whose separation in wavelength is decreasing with increasing order. This double peak structure has been observed for some specific conditions. One possible explanation for the occurrence of these are the contributions of the short and the long trajectory where each refers to one of the peaks.

In the following the influence of the iris diameter, the lens position, the compressor setting, the gas medium and finally the focal length on the harmonic spectra or single harmonic peaks will be investigated.

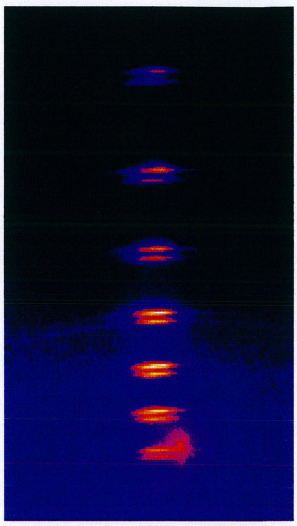

Figure 4.5: Harmonic spectrum consisting of double peaks

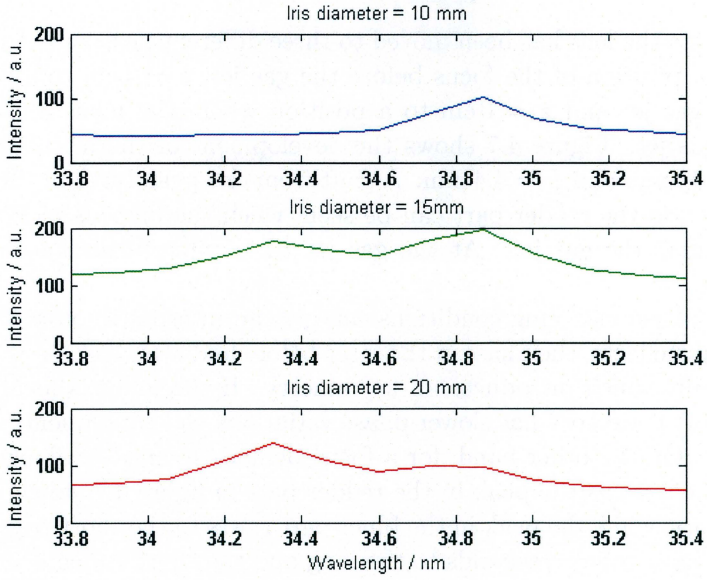

Figure 4.6: Integrated spectrum of the 23^{rd} harmonic order for three different iris diameters

4.2.1 Changing the iris diameter

When increasing the iris diameter, a shift in horizontal direction to the left was observed. This is probably due to an asymmetry in the fundamental beam shape and not shown

here.

A more interesting effect occurs when investigating harmonic spectra consisting of double peaks as the one in figure 4.5. The consideration will now be focused on one harmonic order that is integrated over the horizontal direction of spatial distribution. A such kind of spectrum for the 23^{rd} harmonic order is shown in figure 4.6 with values of $z = 0\,\text{cm}$, $L = 4.4\,\text{mm}$ and three different iris diameters. For $\varnothing = 10\,\text{mm}$ only one peak can be seen. When the iris diameter is increased to 15 mm, a second peak occurs in the bluer part of the spectrum. This refers to the situation in figure 4.5, where the intensities of both peaks are about the same. Increasing the iris diameter further to a value of 20 mm makes the peak in the red part almost disappear and the peak in the bluer part is now clearly the strongest. Thus a specific iris setting can be used to produce either one or the other part of a double peak.

Increasing the iris diameter leads to an increase in intensity of the laser light, and the harmonics are thus produced earlier in time. For a chirped pulse the frequency changes with time and for a negatively chirped pulse the frequencies are higher at the leading edge of the pulse. Thus a shift to wavelengths lying in the blue part as shown in figure 4.6 can be explained.

4.2.2 Influence of the lens position

In the experiments the lens has been moved to three different positions. Here $z = -4\,\text{cm}$ corresponds to a position of the focus before the gas jet, $z = 4\,\text{cm}$ to a position of the focus after the gas jet and $z = 0\,\text{cm}$ to a position where the focus almost lies in the middle of the gas jet. Figure 4.7 shows the development of the intensity for the 23^{rd} order with $\varnothing = 15\,\text{mm}$ and $L = 4.4\,\text{mm}$. A shift from one peak lying in the bluer part to another one lying in the redder part can be seen, when the focus is moved from before the gas jet to after the gas jet. At the gas jet the double peaks known from before appear.

Considering phase matching conditions can give an interpretation of this effect. Neglecting ionization effects, the phase of the laser before and after the gas jet is dominated by the Guoy shift, which introduces an asymmetry. If the focus is located before the medium, the short trajectory has slower phase variations and consequently is selected by phase matching. On the other hand, for a focus behind the medium longer trajectories are phase matched. Thus the peak in the redder part in figure 4.7 would correspond to the long trajectory, while the peak in the bluer part refers to the short trajectory. Which of the peaks in figure 4.5 corresponds to the long and the short trajectory, cannot really be seen. Figure 4.8 shows, however, the 23^{rd} order for the focus at the gas jet, but with an increased iris diameter of 20 mm. It reveals that the peak corresponding to the long trajectory in fact is shifted to longer wavelengths compared to the short trajectory. The long trajectory is characterized by a large divergence, while the peak due to the short trajectory is more concentrated to the center.

Figure 4.9 depicts a plot that is similar to figure 4.7, but now for a positive chirp. Again a shift of the peak can be observed, when moving the focus from before the gas jet to after the gas jet, but the interesting aspect is that it is shifting to shorter wavelengths

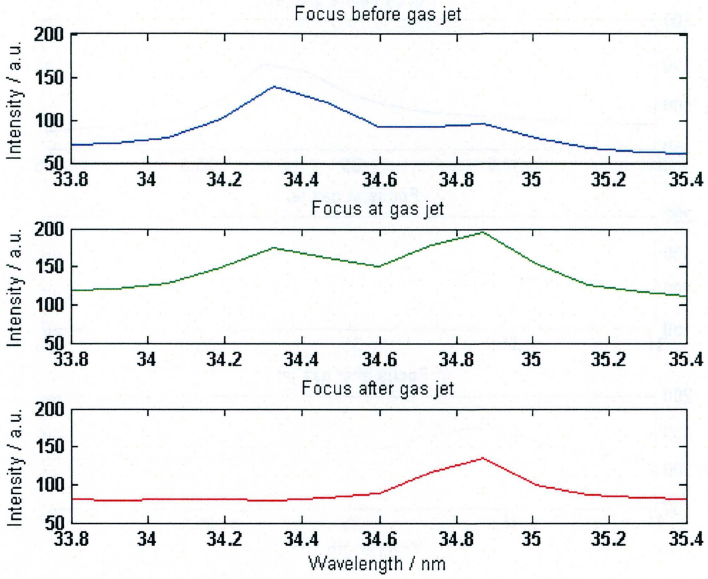

Figure 4.7: Influence of the lens position on the 23^{rd} harmonic order for $L = 4.4\,\mathrm{mm}$

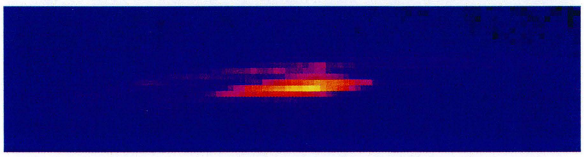

Figure 4.8: 23^{rd} harmonic order for $L = 4.4\,\mathrm{mm}$

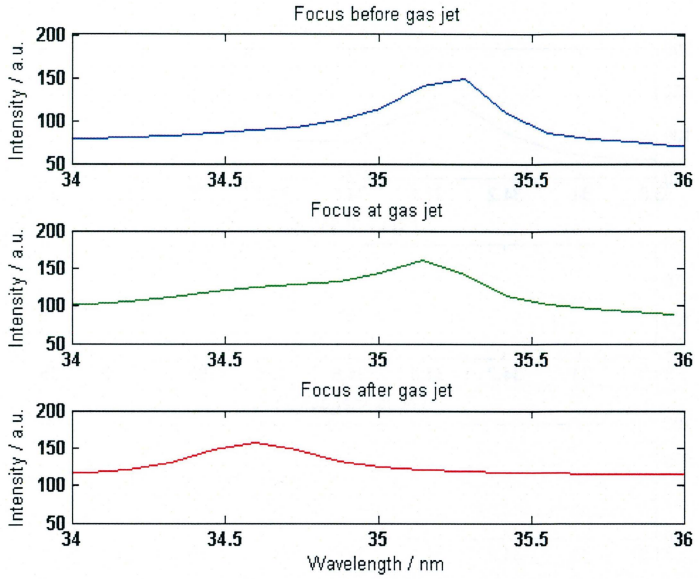

Figure 4.9: Influence of the lens position on the 23^{rd} harmonic order for $L = 6.4\,\mathrm{mm}$

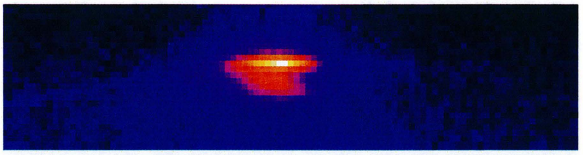

Figure 4.10: 23^{rd} harmonic order for $L = 6.4\,\mathrm{mm}$

now in contrast to the previous case. According to the considerations above, the peak corresponding to the long trajectory should be in the bluer part of the spectrum. Figure 4.10 that shows the 23^{rd} order for the focus at the gas jet and an iris diameter of 15 mm, gives at least some evidence. Besides the upper peak that probably corresponds to the short trajectory, a lower part can be seen that is not that sharp in wavelengths and may refer to the long trajectory.

4.2.3 Variation of the chirp

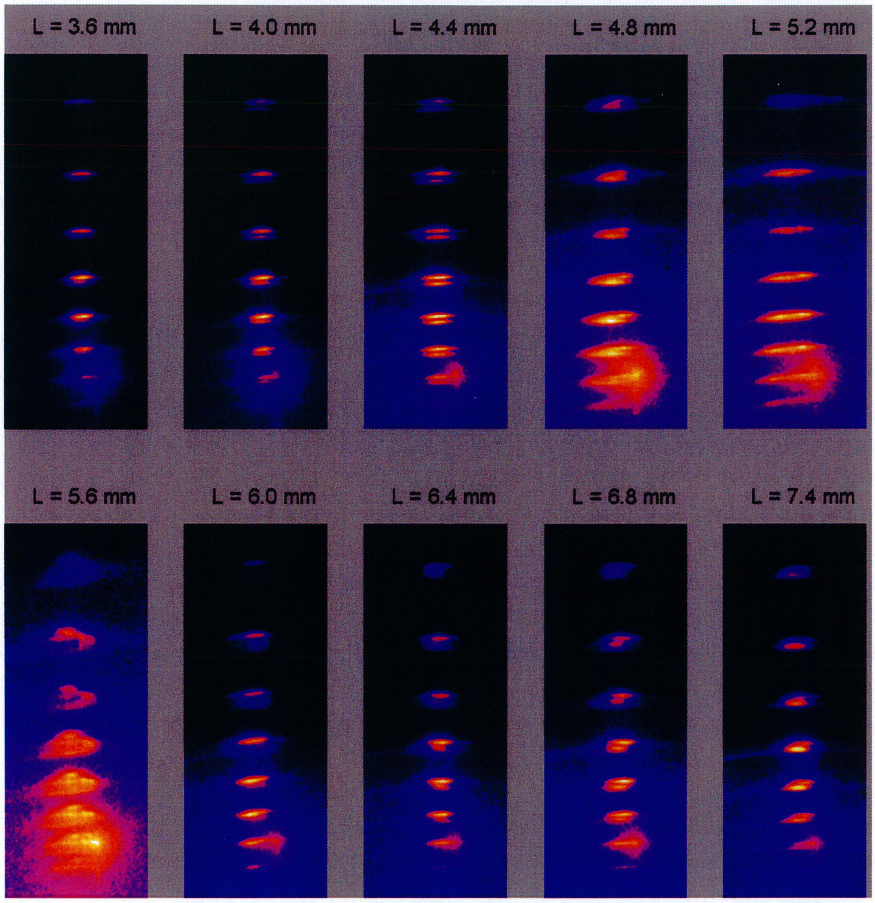

Figure 4.11: Harmonic spectra for different compressor settings

Figure 4.11 shows the evolution of a harmonic spectrum for different compressor settings going from negatively chirped pulses to positively chirped pulses. For $L = 3.6\,\text{mm}$ mainly one sharp peak emerges for each harmonic, whereas for $L = 4.0\,\text{mm}$ and especially for $L = 4.4\,\text{mm}$ the double peak structure can clearly be seen. For $L = 4.8\,\text{mm}$ these two peaks seem to merge getting broader in spectrum and more divergent so that

for $L = 5.2\,\text{mm}$ only one peak occurs. For $L = 5.6\,\text{mm}$ which refers to the shortest pulse duration, the spectrum consists of spectrally very broad harmonics where each seems to be the sum of several contributions. A big change can be seen for $L = 6.0\,\text{mm}$ where the harmonics are sharp again. For $L = 6.4\,\text{mm}$ and $L = 6.8\,\text{mm}$ a second peak becomes visible and for $L = 7.4\,\text{mm}$ the intensity seems to shift to this second peak which is now stronger than the other one.

An explanation why the peak corresponding to the long trajectory is lying on one side compared to the peak corresponding to the short trajectory for a negative chirp, and lying on the other side for a positive chirp, could be found in the simulation that is shown in figure 3.4. For a negative chirp, the blue frequencies travel ahead of the red frequencies. The short trajectory that is generated first, will thus consist of shorter wavelengths compared to the long trajectory that is produced later being in agreement with figure 4.8. On the other side, for a positive chirp where the red frequencies come first, the long trajectory will be moved to higher energies in comparison to the short trajectory (figure 4.10). The upper part of figure 4.11 can thus be interpreted such that there is a maximal separation of the double peaks for a compression of $L = 4.4\,\text{mm}$. For smaller values of L the intensity decreases and this makes both peaks being generated more at the maximum of the dipole phase thus coming closer. For larger values of L, however, the chirp of the laser pulse is reduced and in spite of larger separation in time the beam does not change its frequency very much in time. This leads to the effect that the long and the short trajectory fall together and appear as one sharp peak for $L = 5.2\,\text{mm}$. A similar development can be seen for the lower part of figure 4.11 where the maximum of separation appears for $L = 6.8\,\text{mm}$.

In order to analyze the spectral variation, figure 4.12 shows plots for the 23^{rd} harmonic under the same compressor settings as in figure 4.11. If one concentrates on the peak in the red part, a shift to longer wavelengths can be observed until about $L = 6.0\,\text{mm}$. Then the peak stays about at the same position, but for a value of $L = 7.4\,\text{mm}$ a shift back to shorter wavelengths can be seen. Changing the chirp thus makes it possible to shift the peak in a region of about 1 nm. In comparison to that, the separation to a neighboring harmonic is about 3 nm.

According to the interpretation above, a movement of the harmonics from blue to red wavelengths can be explained by the fact that the leading edge of the laser pulse is changing from blue to red wavelengths when increasing L, and this leading edge is supposed to generate harmonics. There are, however, also other effects as a decreasing intensity that shifts the harmonic generation more to the middle of the pulse. That is why the peak is moving back to blue wavelengths for $L = 7.4\,\text{mm}$.

4.2.4 HHG using Neon

As mentioned before, some experiments have been carried out using Neon as the gaseous medium. The analysis of the taken spectra has not been driven very far, but nevertheless some aspects of high-order harmonic generation are worth pointing out. A harmonic spectrum is depicted in figure 4.13 taken with $\varnothing = 17.5\,\text{mm}$ and $z = -2\,\text{cm}$, which turned out to be the best conditions, as well as $L = 4.4\,\text{mm}$. It includes harmonic orders

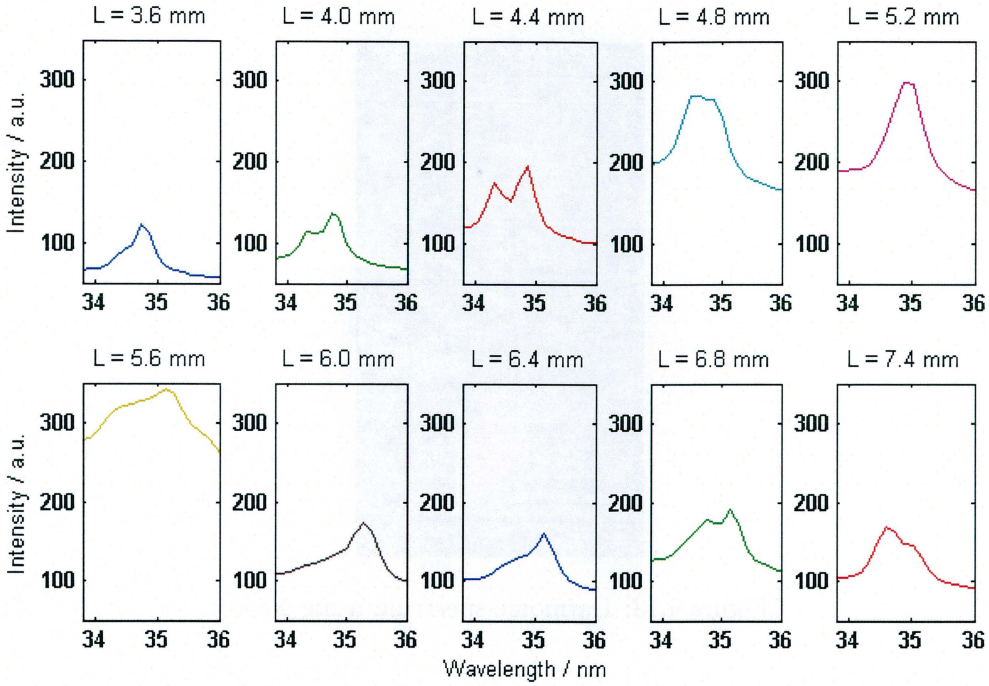

Figure 4.12: 23^{rd} harmonic for different compressor settings

from 19 to 37 and one can see that the peaks lie closer to each other than for Argon. On the other hand, the peaks are weaker now in agreement with the predictions. Even some double peaks occur, but the intensities of the two peaks are more different than before. In addition the separation between the two peaks is smaller now.

The highest order that was observed during the measurements was 47 corresponding to a wavelength of 17 nm. Neon thus enables to go to higher energy harmonic radiation.

4.2.5 HHG using a parabolic mirror

Some spectra were taken using the parabola with a focal length of 1 m in order to have a comparison to the spectra taken before. The spectrum in figure 4.14 refers to the conditions of $\varnothing = 15\,\text{mm}$, $z = 0\,\text{cm}$ and $L = 4.0\,\text{mm}$ using Argon. The divergence of the harmonics is larger now which can be explained by the smaller focal length leading to a smaller beam size in the focus. Thus the harmonics are produced in a smaller volume so that the divergence increases. The conditions for generating harmonics are now not as good due to the smaller interaction volume. Furthermore the intensity now increases faster when approaching the focal point. These effects lead to harmonic radiation with a lower intensity.

Again double structures appear with the more divergent peak lying in the redder

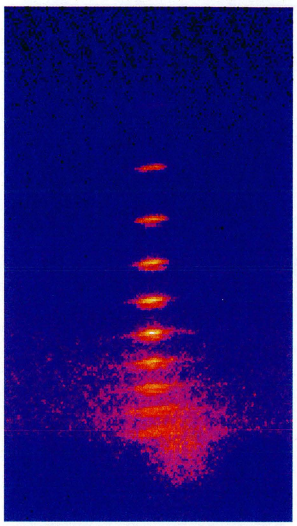

Figure 4.13: Harmonic spectrum using Neon

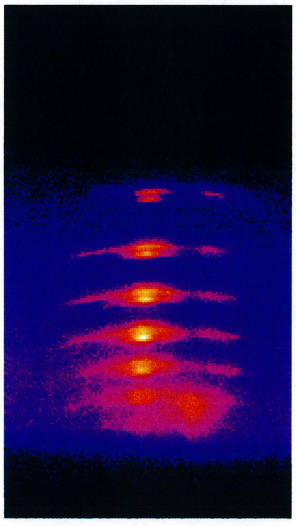

Figure 4.14: Harmonic spectrum using a parabolic mirror

part of the spectrum. This is the same as for negatively chirped pulses using the lens. Investigations also have shown that by changing the iris diameter and the lens position similar effects as in the case before occurred.

Chapter 5

Conclusion and Outlook

During this project a number of parameters have been varied for optimizing harmonic radiation. An accent was put on the occurrence of double peaks and more complicated structures that have not been studied in such details in Lund before. Explanation could be given by referring these structures to the different trajectories of harmonic generation. It was also shown that a tunability of the harmonics could be achieved in a magnitude of about one third of the harmonic spectrum. By changing either the iris diameter or the lens position it is easily possible to select one desired part of a double peak.

The amount of data taken and effects occurring was by far too much in order to be included in the report and my project in general. A model is now being developed to obtain full explanations and simulations are being carried out. This report intends to be a help for these further investigations.

In order to improve the harmonic generation in terms of intensity and tunability, a new setup is now being built. A part of the laser beam referred to as ω will be converted into its second harmonic corresponding to $2\,\omega$. Both ω and $2\,\omega$ combined will then be used to produce harmonics. It has been shown [13] that using the laser beam together with its second harmonic for generating high-order harmonics, results in a much higher conversion efficiency for the harmonics. In addition to the odd harmonics also even harmonics can be observed, which reduces the frequency differences between two harmonics. Furthermore it is expected that by chirping just ω or $2\,\omega$, a high tunability of the generated harmonics can be achieved, possibly over the full harmonic spectrum. This radiation can then be used to perform holographic experiments.

Acknowledgements

First of all I would like to thank Olivier Guilbaud. He deserves special attention, because I worked together with him during most of this project and nothing would really have worked without him. He was teaching me a lot about experimental methods and he spent plenty of time for explaining theoretical issues to me or discussing results as well as many other things trying to answer all my questions.

Anne L'Huillier supervised my project and she was a big help in getting theoretical understanding for our experimental results.

Besides always keeping the laser running, I worked together with Emilie Pourtal during the alignment of the parabolic mirror.

Finally I thank Elisavet Georgiadou for doing simulations, Marko Swoboda for sharing figures with me as well as the whole group.

Bibliography

[1] J. Mauritsson. *Temporal Aspects of High-Intensity Laser-Matter Interactions.* PhD Thesis, Lund Institute of Technology, LRAP-312, 2003.

[2] A. McPherson, G. Gibson, H. Jara, U. Johann, T. S. Luk, I. A. McIntyre, K. Boyer and C. K. Rhodes. *Studies of multiphoton production of vacuum-ultraviolet radiation in the rare gases.* J. Opt. Soc. Am. B, 4, 1987.

[3] M. Fajardo. *TABLETOP ULTRA-INTENSE XUV SOURCES FOR FEMTO-BIOLOGY AND RELATED APPLICATIONS.* Project description, 2004.

[4] S. Svanberg, J. Larsson, A. Persson and C.-G. Wahlstrm. *Lund High-Power Laser Facility – Systems and First Results.* Physica Scripta, Vol. 49, 187-197, 1994.

[5] M. Glimtoft. *Contrast Enhancement of Femtosecond Terawatt Laser Pulses by Preamplification and Temporal Pulse Cleaning.* Master's Thesis, Lund Institute of Technology, LRAP-352, 2006.

[6] S. Häßler, M. Swoboda. *Optimization and Application of High-order Harmonics of an Ultrashort Terawatt Laser.* Lund Institute of Technology, LRAP-324, 2004.

[7] O. Svelto. *Principles of Lasers.* 4th edition, Plenum Press, 1998.

[8] L. Roos. *Optimisation and Application of Intense High-Order Harmonic Pulses.* PhD Thesis, Lund Institute of Technology, LRAP-276, 2001.

[9] C. Lyngå. *High-Order Harmonics — Characterisation, Optimisation and Apllications.* PhD Thesis, Lund Institute of Technology, LRAP-248, 1999.

[10] n.n. *Atoms in strong laser fields - Generation of Attosecond pulses.* Laboratory exercise, Lund Institute of Technology, 2005.

[11] E. Benedetti, J.-P. Caumes, G. Sansone, S. Stagira, C. Vozzi and M. Nisoli. *Frequency chirp of long electron quantum paths in high-order harmonic generation.* Optics Express Vol. 14, No. 6, 2006.

[12] S. Kazamias-Moucan. *Optimisation d'une source d'harmoniques d'ordres élevés pour l'optique non-linéaire dans l'extrême UV.* PhD Thesis, Ecole Polytechnique, 2003.

[13] I. J. Kim, C. M. Kim, H. T. Kim, G. H. Lee, J. Y. Park, D. J. Cho and C. H. Nam. *High Efficient High-Harmonic Generation in an Orthogonally Polarized Two-Color Laser Field.* Physical Review Letters, 94, 243901, 2005.